PAPER

Check for updates

Photodegradation of 2,4-DCP in biochar-related environments: impacts of dissolved organic matter and its molecular weight†

Hui Liu,[ab] Xinkai Gong,[a] Linting Zhang,[c] Maocai Shen,[a] Guoxia Yin[a] and Yulai Wang [ID] *[a]

The widespread application of biochar has inevitably led to the release of various amounts of biochar-derived dissolved organic matter (BDOM) and gradual formation of a biochar-related environment, which significantly influences the environmental behaviors of contaminants. However, the impacts of BDOM on chlorophenol photodegradation remain unknown. In this study, we prepared BDOM from crop residue biochar to evaluate its effects on 2,4-DCP photodegradation. The results showed that 2,4-DCP undergoes self-sensitized photodegradation *via* the self-production of $^1O_2$ and $\cdot$OH in the absence of BDOM. The BDOM enhanced 2,4-DCP photodegradation owing to the production of $^3BDOM^*$, $^1O_2$ and $\cdot$OH, contributing 60%, 22.2% and 4.4%, respectively. Nevertheless, this facilitation effect was weakened with increasing BDOM content because of the enhanced light screening and quenching effects. Low molecular weight (MW, <1 kDa) fractions predominated in BDOM, with a contribution of 62.7%; moreover, these fractions had a higher potential to produce $^3BDOM^*$ and $^1O_2$ and played more important roles in 2,4-DCP indirect photodegradation than high MW fractions. The high MW fractions (MW > 1 kDa) exhibited a stronger light screening effect that decelerated the photodegradation of 2,4-DCP. Furthermore, the degradation of 2,4-DCP by $^3BDOM^*$ occurred *via* both energy and electron transfer pathways, in which low MW fractions of BDOM were predominantly formed *via* the energy transfer pathway, while high MW fractions were mainly formed through the electron transfer pathway. These results suggest that the low MW fractions of BDOM have stronger photoactivity and may play more significant roles in influencing the environmental behaviors of refractory pollutants.

1. Introduction

As a typical class of persistent toxic compounds, chlorophenols can cause damage to multiple organs and endocrine systems in both human and aquatic biota, posing significant eco-environmental risks.[1,2] These compounds are widely used as herbicides, fungicides and pesticides in agriculture.[3,4] In the natural environment, chlorophenols can persist for up to 28 years due to their resistance to biodegradation.[5] Accordingly, chlorophenols and their byproducts, such as 2,4-dichlorophenol (2,4-DCP), are frequently detected in seawater, drinking water and surface water, with concentrations reaching as high as 10 μg L^{-1}.[6,7] Owing to the overlapping absorption

bands of chlorophenols and the tropospheric solar spectrum, these compounds are considered to undergo photolysis in natural environments. The photolysis of chlorophenols generally involves direct and indirect photodegradation. Direct photodegradation primarily depends on the chemical structure of chlorophenols, whereas indirect photodegradation is largely influenced by coexisting substances, particularly photosensitizers.[8]

The increasing global population and rising food demand have led to the production of a large amount of agricultural straws and other residues (up to 5 billion tons per year), such as rice husk, corn stover, wheat straw and cotton straw.[9,10] Returning crop residues into soil by converting them into biochar is a promising approach for maximizing their utilization, including enhancing soil fertility, reducing environmental pollution and sequestering carbon.[11–13] Intensive research has shown that biochar has great remediation potential for pesticide-contaminated soil because of the following reasons: (i) it displays a remarkable adsorption affinity towards pesticides due to its strong hydrophobicity and (ii) it usually has abundant surface functional groups and superior pore structure, which facilitate the adsorption of pesticides through

[a]School of Energy and Environment, Anhui University of Technology, Maanshan City 243002, China. E-mail: yulai_wang@163.com

[b]State Key Laboratory of Pollution Control and Resource Reuse, School of the Environment, Nanjing University, Jiangsu, 210046, China

[c]Fujian Provincial Key Laboratory of Island Conservation and Development, Island Research Center, Ministry of Natural Resources, Pingtan Comprehensive Pilot Zone, 350400, China

† Electronic supplementary information (ESI) available. See DOI: https://doi.org/10.1039/d5ra02462e

hydrogen bonding, pore filling, electrostatic attractions, and van der Waals forces.[14,15] The widespread application of biochar can lead to the significant infiltration of biochar-derived dissolved organic matter (BDOM) into agricultural watersheds through leaching and surface runoff.[16,17] Consequently, biochar-related environments, such as biochar-based biofiltration systems, have been developed.[18] Additionally, crop residues are rich in cellulose, hemicellulose and lignin.[19] Biochar derived from crop residues usually contains amounts of BDOM, especially those produced through hydrothermal processes or pyrolysis at low temperatures.[20,21] Compared with biochar particles, BDOM exhibits stronger motility, lower hydrophobicity and smaller molecular size, enabling it to be readily released in biochar-related environments and significantly influence the transformation of chlorophenols.[22,23]

Current research has demonstrated that BDOM is a typical photosensitizer and exhibits stronger photoactivity than natural DOM.[24] BDOM can generate multiple reactive oxygen species (ROS) under solar irradiation, such as triplet-excited states of BDOM (^{3}BDOM*), singlet oxygen ($^1O_2$), hydroxyl radical ($^•$OH) and superoxide radical ($O_2^{•-}$).[3,24] The quantum yields of ^{3}BDOM* and $^1O_2$ generated by BDOM were 4–8 times and 2–3 times higher than many reported DOMs, respectively.[25,26] However, BDOM can decrease light absorption by combining with pollutants or scavenging the excited states of pollutants and ROS, resulting in decreased photoirradiation efficiency.[27] In parallel, it has been reported that the antioxidants in BDOM, such as phenolic moieties, can inhibit triplet-induced photodegradation.[28,29] Furthermore, BDOM consists of various organic molecules with different molecular weights (MW).[30] As a heterogeneous mixture, the MW of BDOM is one of the most important factors determining its environmental behavior.[31–33] It has been reported that the photochemical reactivity of BDOM is highly dependent on its molecular size.[34–37] Therefore, it is reasonable to assume that the photodegradation process of chlorophenol would be significantly influenced by BDOM and varies with the MW fraction.

To investigate the impact mechanisms of a previously overlooked significant component during the application of biochar, namely BDOM, on the photodegradation of pollutants, this study innovatively proposes the scientific hypothesis that "BDOM would alter the photodegradation process of chlorophenol pesticides, and this alteration is dependent on the MW fractions of BDOM because of their differences in producing various species and quantities of ROS". To validate this hypothesis, we prepared BDOM from crop residue biochar and divided it into three MW fractions, along with evaluating their impacts on 2,4-DCP photodegradation. The primary aims of this study were to (1) investigate the photodegradation process of 2,4-DCP mediated by BDOM and its MW fractions; (2) determine the primary ROS and reveal their roles in chlorophenol photodegradation systems; and (3) understand the underlying mechanisms of BDOM-mediated chlorophenol photodegradation. These results are valuable for understanding the mechanisms of BDOM-mediated chlorophenol photodegradation in biochar-related environments.

2. Materials and methods

2.1 Chemicals and materials

2,4-DCP and 2,2′-azino-bis(3-ethylbenzothiazoline-6-sulfonic acid)diammonium salt (ABTS) were purchased from Aladdin Industrial, Inc. (Shanghai, China). All the chemicals used in this study were of analytical grade and were used without further purification. All solutions were prepared using ultrapure water.

2.2 Biochar, BDOM preparation and MW fractions

Biochar and BDOM were prepared as described in our previous work.[38] Briefly, cotton straw was collected, washed with deionized water, dried at 80 °C for 24 h and ground into powder. Cotton straw powder was hydrothermally carbonized at 220 °C for 4 h to obtain biochar. Then, 5 g of biochar was suspended in 100 mL of deionized water in a sealed container, which was shaken at 25 °C for 24 h. Finally, bulk-BDOM was obtained by filtering the suspension through a 0.45 μm PVDF.

The BDOM fractions with different MWs were prepared using the ultrafiltration procedure according to the literature.[33,39] In brief, bulk-BDOM was sequentially filtered through 1 kDa and 5 kDa filter membranes. Consequently, the bulk-BDOM was divided into three fractions with the MW < 1 kDa, 1 kDa < MW < 5 and MW > 5 kDa, which were named low MW BDOM (L-BDOM), medium MW BDOM (M-BDOM) and high MW BDOM (H-BDOM), respectively.

2.3 Photodegradation experiments

The 2,4-DCP photodegradation experiments were conducted in a photoreactor equipped with a UVB-313 lamp (15 W) and a UVA-340 lamp (15 W). The initial pH was kept at 6.5 ± 0.2 using NaOH or H_2SO_4 at a reaction temperature of 25 °C. Typically, BDOM was added to 5 L of 2,4-DCP solution at an initial concentration of 5 mg L^{-1}. The reaction container was placed approximately 5 cm beneath the UV lamps. The radiation intensity at the solution was 2.63 W m^{-2} for UVA and 1.05 W m^{-2} for UVB, approximately 50 times the summer sunlight dose in Hefei City.[40] The solution was continuously stirred and samples were withdrawn at preset intervals. The samples were immediately filtered through a 0.45 μm PVDF membrane for testing the 2,4-DCP concentration. The dark control experiments were conducted under the same conditions, except for UV irradiation. All experiments were conducted in triplicate. The photodegradation of 2,4-DCP dynamics was analyzed according to the pseudo-first-order kinetic model described by eqn (1).[41]

$$\ln(C_t/C_0) = -k_{obs}t, \quad (1)$$

where C_t (mg L^{-1}) is the concentration of 2,4-DCP at t and C_0 (mg L^{-1}) is the initial concentration of 2,4-DCP. k_{obs} (h^{-1}) is the observed pseudo-first-order rate constant.

The indirect photolysis rate constant (k_{ind}) induced by BDOM was calculated based on the total light screening factors ($\sum S_\lambda$) according to the following equations:[32,42]

$$S_\lambda = \frac{1 - 10^{-a_\lambda l}}{2.303 l a_\lambda}, \qquad (2)$$

$$\sum S_\lambda = \frac{\sum I_\lambda S_\lambda \varepsilon_\lambda}{\sum I_\lambda \varepsilon_\lambda}, \qquad (3)$$

$$k_{ind} = k_{obs} - k_d \sum S_\lambda, \qquad (4)$$

where α_λ (cm^{-1}) is the corrected light attenuation coefficient at λ (cm). ε_λ (L cm^{-1} mol^{-1}) is the molar absorptivity of the reactant, and l (cm) is the light path length. k_{ind} and k_d (h^{-1}) are the photolysis rates with and without BDOM, respectively.

2.4 Quenching experiments

The roles of ROS on 2,4-DCP photodegradation were investigated *via* quenching experiments. Based on our preliminary experiments, 0.56 g per L sorbic acid (SA) and 0.70 g per L TMP were used as the quencher of ^{3}BDOM*, while 6.0 g per L isopropyl alcohol (IPA) and 1.0 g per L furfuryl alcohol (FFA) were chosen as the quencher of ˙OH and ^{1}O$_2$, respectively.

The steady-state concentrations of ^{3}BDOM* ([^{3}BDOM*]$_{ss}$) and ^{1}O$_2$ ([^{1}O$_2$]$_{ss}$) were determined using 2,4,6-trimethylphenol (TMP) and FFA as chemical probes, respectively. The [^{3}BDOM*]$_{ss}$ and [^{1}O$_2$]$_{ss}$ were calculated as follows:[43]

$$\left[^3\text{BDOM}^*\right]_{ss} = \frac{k_{obs,TMP}}{k_{^3BDOM^*,TMP}}, \qquad (5)$$

$$\left[^1\text{O}_2\right]_{ss} = \frac{k_{obs,FFA}}{k_{^1O_2,FFA}}, \qquad (6)$$

where $k_{obs,FFA}$ (s^{-1}) and $k_{obs,TMP}$ (s^{-1}) are the degradation rates of FFA and TMP, respectively. $k_{^3BDOM^*,TMP}$ is the second-order reaction rate constants between ^{3}BDOM* and TMP, which is 3.0×10^9 M^{-1} s^{-1}. $k_{^1O_2,FFA}$ is the second-order reaction rate constant between ^{1}O$_2$ and FFA, which is 1.0×10^8 M^{-1} s^{-1} according to Appiani *et al.*[44]

2.5 Analytical methods

The mineral composition of biochar was characterized by X-ray fluorescence (XRF) (Thermo Fisher Scientific, USA). The specific surface area of biochar was calculated by the Brunauer–Emmett–Teller (BET) method from N$_2$ gas physisorption isotherms using an ASAP 2020 instrument (ASAP 2460, Micromeritics, USA) at −196 °C (77 K). The pore volume of biochar was measured using the Barrett–Joyner–Halenda (BJH) method. The FT-IR spectra of the biochar were obtained using a Nicolet 670 FT-IR spectrometer.

The MW distribution of bulk-BDOM was detected using a GPC analyzer (1206, Agilent, USA) equipped with a GPC column (Waters Ultrahydrogel, 300 × 7.8 mm, 500–250–120 Å) and a UV detector. A phosphate buffer solution was used as the mobile phase at pH 7.4 and a flow rate of 1 mL min^{-1}. The known MW polyethylene glycols were used as the standard solutions. The concentrations of bulk-BDOM and its MW fractions (mg C per L as DOC) were quantified using a total organic carbon (TOC) analyzer (Shimadzu, Japan). The UV-vis

absorption spectra of BDOM were measured using a TU-1901 spectrophotometer, and the FT-IR spectra of BDOM were obtained on a Nicolet 670 FT-IR spectrometer.

The ROS generated during the BDOM-mediated photodegradation of 2,4-DCP was detected using electron paramagnetic resonance (EPR, EMXplus-6/1, Bruker, Germany). The 2,2,6,6-tetramethylpiperidine (TEMP) and 5,5-dimethyl-1-pyrroline-*N*-oxide (DMPO) spin probes were used to capture the generated ^{1}O$_2$ and ˙OH, respectively.[13]

The electron-donating capacity (EDC) of bulk-BDOM and its MW fractions was measured by mediated electrochemistry using a CHI670E electrochemical workstation in a three-electrode system according to the literature.[29,45] A glassy carbon cylinder was used as the working electrode and electrochemical reactor. The reference electrode and counter electrode were Ag/AgCl and platinum wire, respectively. Briefly, 9 mL of 0.1 M phosphate buffer (pH = 7) with 0.1 M KCl was added into the cell, and the solution was continuously purged with an N$_2$ flow to remove dissolved oxygen. The redox potential was set at +0.61 V using the ampere *i*–*t* curve method, and then 100 μL of ABTS (10 mM) was added to the solution to establish an oxidation–reduction equilibrium. When the background current reached equilibrium, 100 μL of BDOM was spiked into the reactor. The electron transfer numbers from the BDOM to the working electrode were determined by integrating the current peak response, and the EDC values of the BDOM were calculated using the following equation:[45–47]

$$\text{EDC} = \frac{\int I_{ox}/F dt}{m_{BDOM}}, \qquad (7)$$

where I_{ox} (A) is the baseline-corrected oxidative current. F (96 485 C mol^{-1}) is the Faraday constant. m_{BDOM} (g DOC) is the carbon content in the reaction system.

The 2,4-DCP, FFA and TMP concentrations were determined using high-performance liquid chromatography (EX-1800, Wufeng, China) equipped with a Zorbax SB-C18 with detection wavelengths of 280, 216 and 220 nm, respectively. The mobile phase of 2,4-DCP was water/acetonitrile (20/80, v/v). The mobile phase for FFA and TMP consisted of water (0.1% phosphoric acid) and acetonitrile at ratios of 90 : 10 (v/v) and 55 : 45 (v/v), respectively. The intermediates of 2,4-DCP produced during the photodegradation process were identified using a GC/MS (TRACE1300, Thermo Fisher Scientific, USA) equipped with a DB-5MS capillary column (30 m × 0.25 mm, 0.25 μm). The sample obtained during the 2,4-DCP photodegradation process was extracted using dichloromethane. The extracted sample was injected at 270 °C using the splitless mode with a 1.0 L per min helium flow as the carrier gas. The initial temperature was set to 40 °C. It was then ramped up to 100 °C with a 12 °C min^{-1} rate, followed by an increase to 200 °C with a 5 °C min^{-1} rate, finally raised to 270 °C with a 20 °C min^{-1} rate and held for 5 min.

3. Results and discussion

3.1 The initiation of 2,4-DCP degradation

Under dark conditions, the observed concentrations of 2,4-DCP remained stable, both in the presence and absence of BDOM
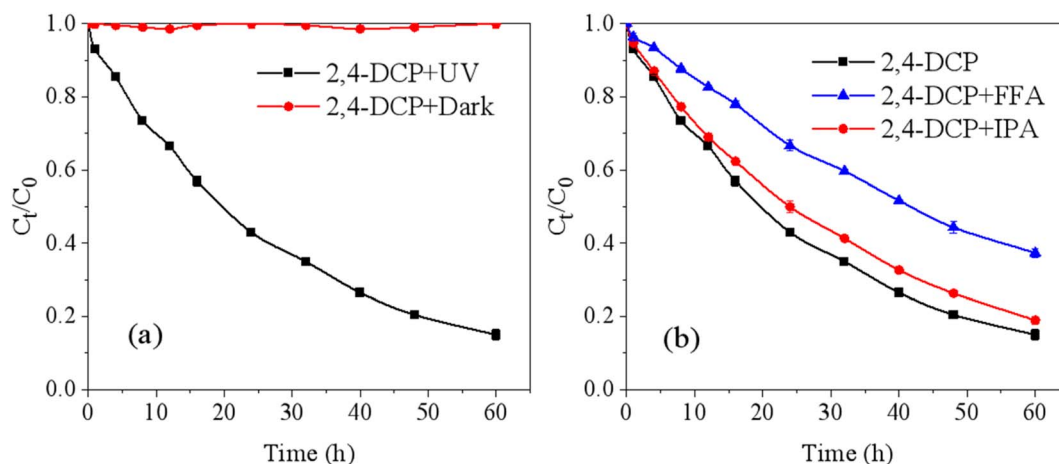
Fig. 1 (a) Photodegradation of 2,4-DCP in pure water and (b) its quenching experiment using FFA and IPA. Experimental conditions: 2,4-DCP initial concentration: 5 mg L^{-1}; pH 6.5 ± 0.2.

(Fig. S1†), suggesting that the non-photochemical processes affecting 2,4-DCP may be negligible. After 60 h of irradiation, 85% of 2,4-DCP was degraded in the absence of BDOM (Fig. 1a), indicating that UV irradiation was the key factor triggering 2,4-DCP degradation. To explore the indirect photodegradation process of 2,4-DCP, quenching experiments were conducted using FFA and IPA as quenchers for $^1O_2$ and $^{\cdot}OH$, respectively. As shown in Fig. 1b, the degradation of 2,4-DCP was reduced by 12% and 4% after adding FFA and IPA, respectively. The degradation of 2,4-DCP can be accurately described by pseudo-first-order kinetics. The degradation rate calculated based on pseudo-first-order kinetics decreased by 50% and 16% by FFA and IPA, respectively. These findings suggest that $^1O_2$ and $^{\cdot}OH$ play significant roles in 2,4-DCP degradation, and $^1O_2$ exhibits higher activity than $^{\cdot}OH$.[48] It is worth noting that some organic contaminants can self-produce reactive intermediates upon photon absorption, such as their triplet states, which can react with dissolved oxygen to form $^1O_2$ and $^{\cdot}OH$ through electron transfer.[49] Additionally, Fu et al.[50] suggested that the ROS

induced by organic contaminants in turn result in their degradation, a process referred to as self-photosensitization. Accordingly, 2,4-DCP undergoes self-photosensitization mediated by self-produced $^1O_2$ and $^{\cdot}OH$.

3.2 Impact of bulk-BDOM concentration 2,4-DCP photodegradation process

The 2,4-DCP photodegradation curves in the context of bulk-BDOM are shown in Fig. 2a. After UV irradiation for 60 h, 91–96% of 2,4-DCP was degraded in the presence of bulk-BDOM, showing a 6–11% increase in 2,4-DCP degradation efficiency compared to that without BDOM. The photodegradation of 2,4-DCP mediated by bulk-BDOM can be described by pseudo-first-order kinetics, as evidenced by the fitting results (Table S1†). We found that the k_{ind} values at different bulk-BDOM concentrations were positive, and the k_{obs} values of 2,4-DCP photodegradation mediated by bulk-BDOM were higher than those without bulk-BDOM (Fig. 2b). These findings suggest that bulk-
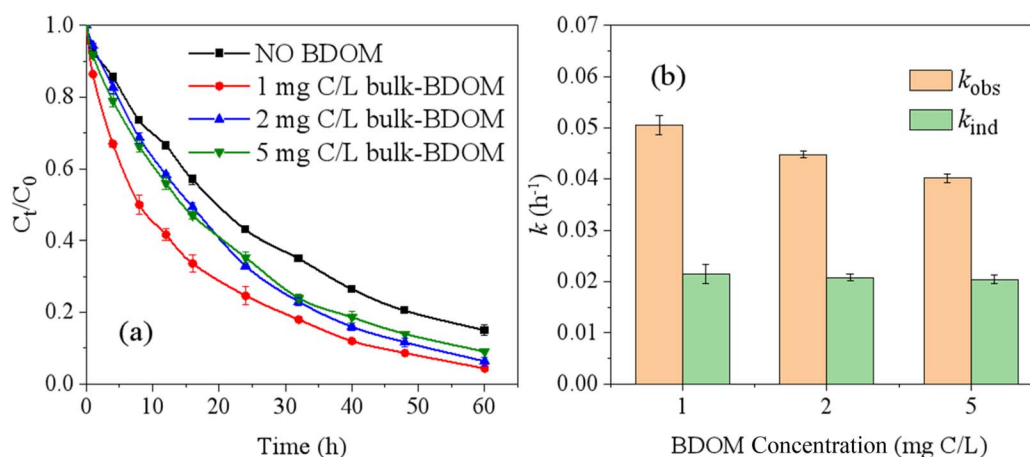

Fig. 2 Photodegradation of 2,4-DCP (a) in the presence of bulk-BDOM and (b) observed photodegradation rates and indirect photodegradation rates of 2,4-DCP at various bulk-BDOM concentrations. Experiment conditions: 2,4-DCP initial concentration: 5 mg L^{-1}; pH 6.5 ± 0.2.

BDOM facilitates the overall photodegradation of 2,4-DCP by improving its indirect photodegradation.

Interestingly, the k_{obs} values decreased from 0.0505 h^{-1} to 0.0402 h^{-1} and the k_{ind} values decreased from 0.0215 h^{-1} to 0.0204 h^{-1}, with the bulk-BDOM concentration increasing from 1 mg C per L to 5 mg C per L. These results indicate that the facilitation effect was weakened by increasing the bulk-BDOM concentration. As shown in Table S1,† the smaller $\sum S_\lambda$ value was observed at higher bulk-BDOM concentrations, suggesting that higher bulk-BDOM concentrations have stronger light screening effects, leading to decreased photoirradiation efficiency. Thus, the weakened facilitation effect of 2,4-DCP overall photodegradation could be partially ascribed to the amplified light screening effect at high bulk-BDOM concentrations.[51] Notably, higher BDOM concentrations usually lead to increased steady-state concentrations of ROS, thereby enhancing indirect photodegradation.[52] However, our results showed that high BDOM concentrations decelerated the indirect photodegradation of 2,4-DCP, which is contrary to previous research. It has been reported that BDOM could serve as a quencher of ^{3}BDOM* at high concentrations,[51] particularly for BDOM derived from crop residues because of its high content of highly unsaturated phenolic compounds (up to 50%) that could inhibit the triplet-induced transformation.[53,54] Accordingly, the decreased indirect photodegradation rate of 2,4-DCP with bulk-BDOM concentration can be attributed to the effective quenching of ROS by phenolic compounds in bulk-BDOM.

To identify the ROS generated during the photodegradation of 2,4-DCP mediated by bulk BDOM, we employed EPR spectroscopy in this study. As shown in Fig. 3, after UV irradiation for 10 min, a 1 : 1 : 1 triplet signal and a 1 : 2 : 2 : 1 quartet signal were observed in the presence of TEMP and DMPO, representing TEMP–^{1}O$_2$ adduct and DMPO–OH adducts, respectively.[55,56] These findings confirm the generation of ^{1}O$_2$ and ·OH during 2,4-DCP photodegradation in the presence of bulk-BDOM. The roles of ROS in the bulk-BDOM-mediated 2,4-DCP photodegradation process were further evaluated using quenching experiments. After the introduction of SA, TMP, FFA and IPA, we observed that the k_{obs} values of 2,4-DCP photodegradation

decreased by 30.3%, 29.7%, 22.2% and 4.4%, respectively (Fig. 4). This result indicates that ^{3}BDOM* plays a dominant role in enhancing 2,4-DCP indirect photodegradation, followed by ^{1}O$_2$, and that the role of ·OH is negligible. Additionally, the quenching of ^{3}BDOM* by SA and TMP is typically related to the electron- and energy-transfer pathways of ^{3}BDOM* in photodegradation reactions.[57,58] The approximated inhibition efficiency by SA and TMP indicated that 2,4-DCP degradation by ^{3}BDOM* occurs *via* both electron- and energy-transfer pathways.

3.3 Impact of BDOM MW fraction on 2,4-DCP photodegradation

The impacts of various BDOM MW fractions on 2,4-DCP photodegradation are shown in Fig. 5. The degradation rates of 2,4-DCP calculated based on the pseudo-first-order kinetics are listed in Table 1. The k_{obs} values of 2,4-DCP in the presence of L-BDOM were 0.0370–0.0464 h^{-1}, higher than those without BDOM, reflecting the facilitation effect of L-BDOM on 2,4-DCP photodegradation. However, the k_{obs} values of 2,4-DCP photodegradation mediated by H-BDOM ranged from 0.0262–0.0328 h^{-1}, displaying an inhibitor effect. Additionally, we found that all $k_{ind}s$ of values were positive, suggesting that each MW fraction of BDOM enhanced the indirect photodegradation of 2,4-DCP. The k_{ind} values for L-BDOM-mediated 2,4-DCP photodegradation were higher than those for M-BDOM and H-BDOM, reflecting that lower MW fractions of BDOM contributed more to the indirect photodegradation of 2,4-DCP. It is noteworthy that the k_{ind} values showed a trend of first increasing and then decreasing with increasing BDOM fraction concentration. These findings suggest that the impact of BDOM on 2,4-DCP photodegradation depends on not only the BDOM concentration but also the MW fraction.

The roles of ROS in 2,4-DCP photodegradation mediated by different BDOM fractions were evaluated in quenching experiments. The k_{obs} values of 2,4-DCP photodegradation in the presence of quenchers, calculated based on the pseudo-first-order kinetic model, are listed in Table S2.† In the 2,4-DCP/L-
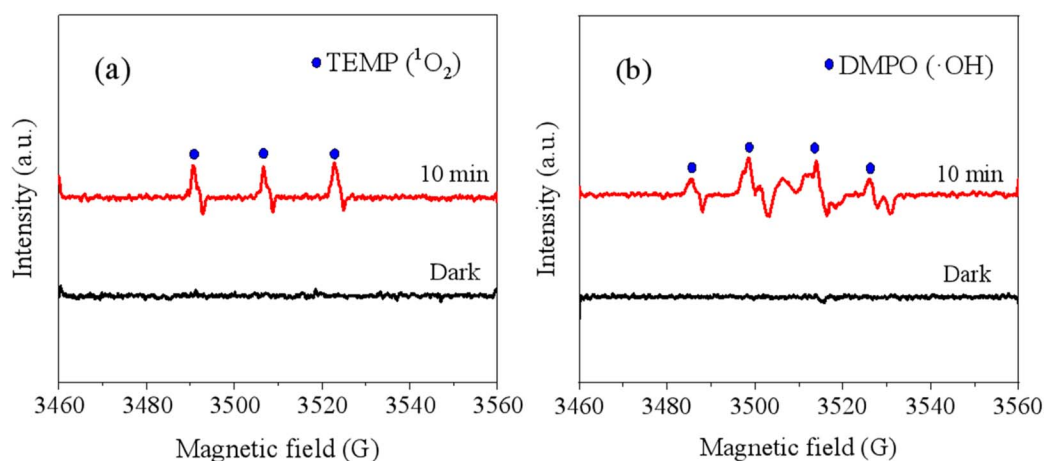

Fig. 3 EPR spectra of (a) TEMP spin adducts and (b) DMPO−OH adducts in the bulk-BDOM/2,4-DCP system after 10 min of irradiation.
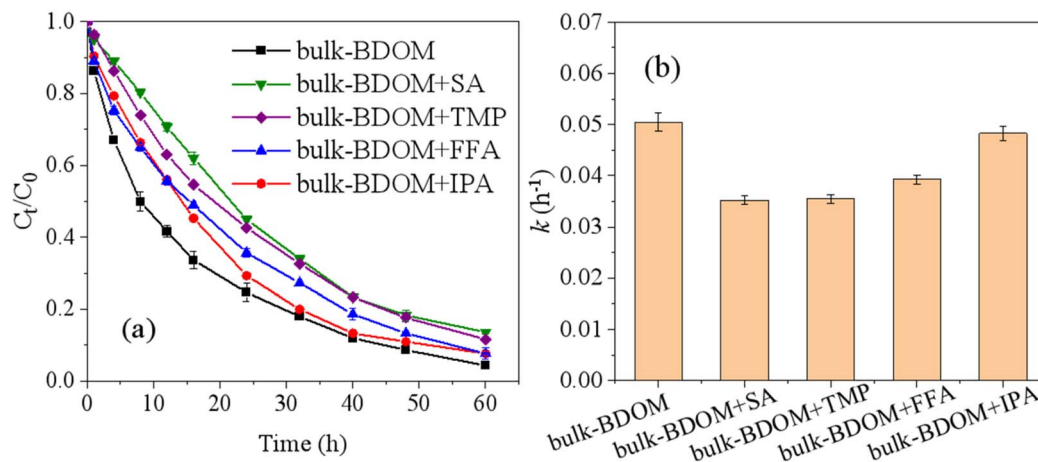
Fig. 4 (a) Quenching experiments of 2,4-DCP in the presence of bulk-BDOM and (b) observed photodegradation rates of 2,4-DCP. Experiment conditions: 2,4-DCP initial concentration: 5 mg L^{-1}; bulk-BDOM concentration: 1 mg per C L; pH 6.5 ± 0.2.

BDOM system, the addition of SA, TMP, FFA and IPA induced the k_{obs} values of 2,4-DCP photodegradation decreased by 56.1%, 25.7%, 49.0% and 40.5%, respectively (Fig. 6a), indicating that ^{3}BDOM* played the dominant role in L-BDOM-mediated 2,4-DCP photodegradation, while $^1O_2$ and ·OH played secondary roles. The stronger inhibitory effect of SA than

TMP indicates that ^{3}BDOM* produced by L-BDOM reacted with 2,4-DCP mainly via an energy transfer pathway.[58] For M-/H-BDOM-mediated 2,4-DCP photodegradation, the introduction of TMP induced the k_{obs} values of 2,4-DCP photodegradation to be reduced by 17.8% and 10.7%, respectively, whereas no obvious change was observed in the presence of SA, FFA and
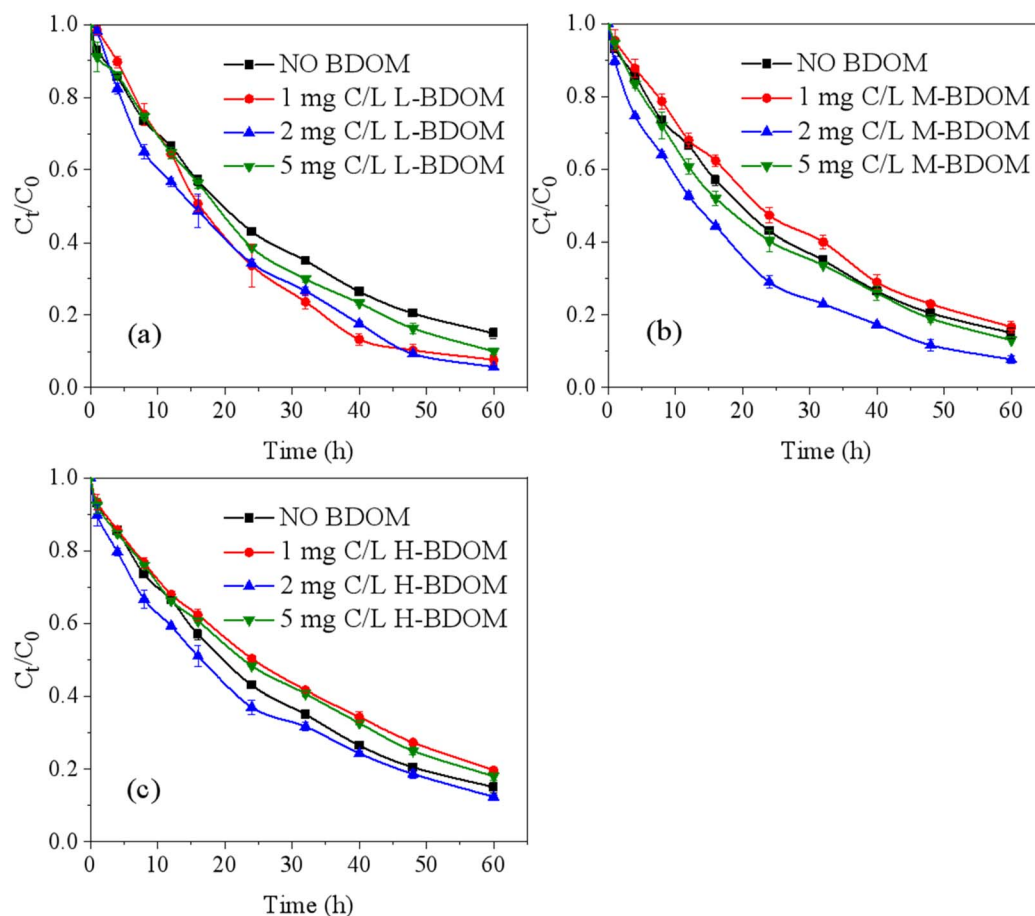

Fig. 5 Photodegradation of 2,4-DCP in the presence of (a) L-BDOM, (b) M-BDOM and (c) H-BDOM. Experiment conditions: pH 6.5 ± 0.2; 2,4-DCP initial concentration: 5 mg L^{-1}.

Table 1 Observed and indirect photodegradation of 2,4-DCP in the presence of various BDOM fractions based on the pseudo-first-order kinetics and their light screening correction factors

BDOM concentration (mg C per L)	BDOM fraction	k_{obs} (h^{-1})	R^2	$\sum S_\lambda$	k_{ind} (h^{-1})
0	NO BDOM	0.0322	0.9976	—	—
1	L-BDOM	0.0435	0.9842	0.5443	0.0260
	M-BDOM	0.0297	0.9974	0.5270	0.0127
	H-BDOM	0.0262	0.9984	0.4966	0.0102
2	L-BDOM	0.0464	0.9944	0.4918	0.0310
	M-BDOM	0.0413	0.9976	0.4706	0.0261
	H-BDOM	0.0328	0.9974	0.4531	0.0182
5	L-BDOM	0.0370	0.9985	0.4585	0.0222
	M-BDOM	0.0335	0.9996	0.4250	0.0198
	H-BDOM	0.0268	0.9977	0.4031	0.0138

IPA. These findings indicate that ^{3}BDOM* preferentially reacted with 2,4-DCP *via* an electron transfer pathway during M- and H-BDOM-mediated photodegradation, with the contributions of $^1O_2$ and ˙OH being negligible.

3.4 The 2,4-DCP photodegradation process mediated by BDOM

The experimental results demonstrated that BDOM facilitates the indirect photodegradation of 2,4-DCP, and this facilitation depends on the concentration and molecular weight of the substrate. The various MW fractions of BDOM may contribute to the dual effect of bulk BDOM on 2,4-DCP photodegradation. To assess the impact of the full molecular weight spectrum of BDOM on 2,4-DCP photodegradation, this study analyzed the spectrum and compositional parameters of BDOM fractions with various MWs. As shown in Fig. 7a, bulk-BDOM exhibited an MW distribution ranging from 0 to 5.8 kDa, with a peak center of 1.2 kDa. The DOC concentrations of the extracted
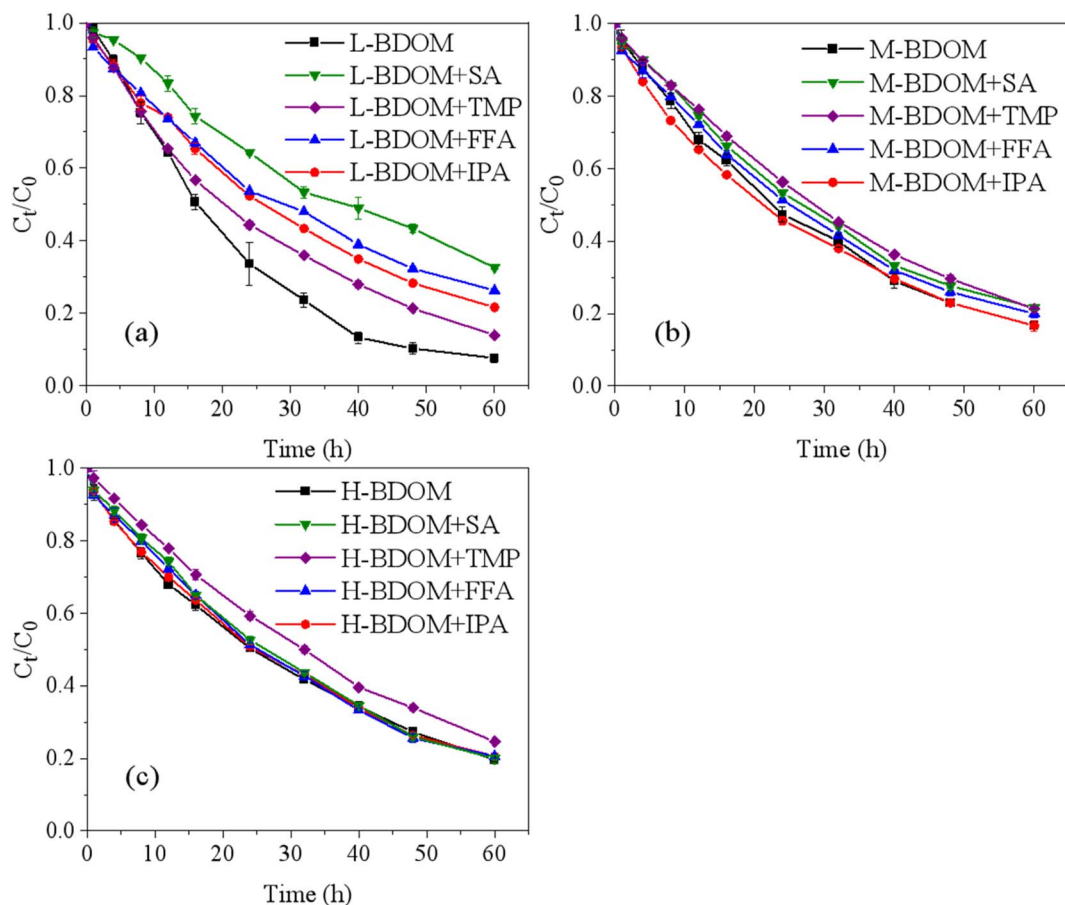

Fig. 6 Quenching experiments of 2,4-DCP photodegradation in the presence of (a) L-BDOM, (b) M-BDOM and (c) H-BDOM. Experiment conditions: BDOM concentration of 1 mg C per L; 2,4-DCP initial concentration: 5 mg L^{-1}; pH 6.5 ± 0.2.
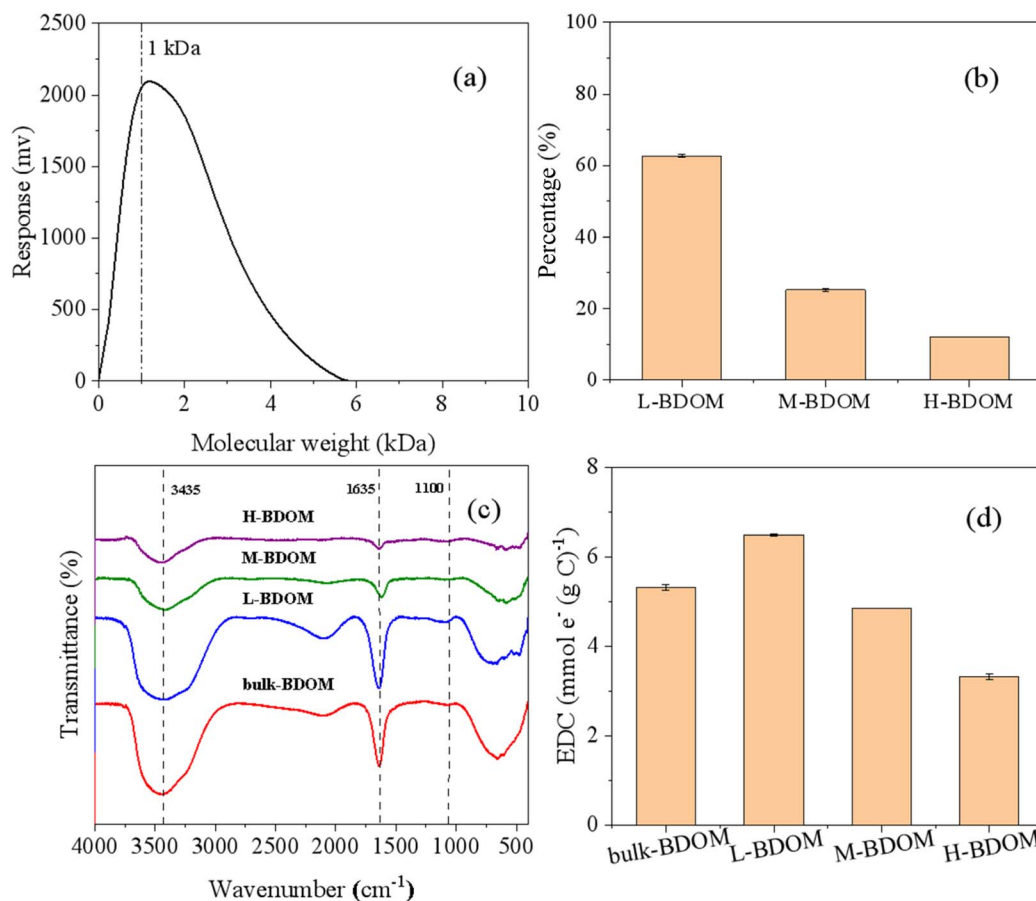
Fig. 7 (a) Molecular weight distribution of BDOM, (b) proportion of each MW fraction in bulk-BDOM, (c) FT-IR spectra and (d) electronic supply capability of bulk-BDOM and its molecular weight fractions.

bulk-BDOM and its MW fractions are listed in Table S3.† After grouping the BDOM into three MW fractions, the recovery of BDOM was 93.6%, as determined by calculating the DOC concentration. The percentages of L-BDOM, M-BDOM and H-BDOM contributing to bulk-BDOM were 62.7%, 25.3% and 12.0%, respectively (Fig. 7b). This showed that the BDOM fraction with MW < 1 kDa was predominant in bulk-BDOM, followed by the MW range of 1–5 kDa and MW > 5 kDa.

The indirect photodegradation is related to the ROS derived from BDOM. Thus, the steady-state concentrations of ^{3}BDOM* and $^1O_2$ produced by the BDOM MW fractions were determined in this study and listed in Table 2. The results showed that $[^3\text{BDOM*}]_{ss}$ and $[^1O_2]_{ss}$ produced by the three BDOM fractions followed the order of L-BDOM > M-BDOM > H-BDOM, which suggested that the lower MW fractions in BDOM contributed to more ROS. This result explains the higher indirect

photodegradation of 2,4-DCP observed at lower BDOM MW fractions. The variations in ROS derived from the three BDOM fractions are attributed to differences in their composition and structures. As shown in UV-vis absorption spectra (Fig. S3†), L-BDOM displayed a shoulder peak with a wavelength range of 250–300 nm, which was generally related to the π–π electron transition of the C=C and C=O double bond groups.[59] The FT-IR spectra of bulk-BDOM and its MW fractions (Fig. 7c) showed a similar shape curve, reflecting similar types of functional groups for bulk-BDOM and its MW fractions. Nevertheless, the intensity of the characteristic peak at 1635 cm^{-1} corresponding to C=O stretching vibration followed the order of L-BDOM > M-BDOM > H-BDOM, reflecting a higher carbonyl content of the lower MW fraction.[60] Previous studies have reported that aromatic carbonyls such as aldehyde, ketone and quinones are important precursors of ^{3}BDOM*,[48] and ^{3}BDOM* further reacts

Table 2 Steady-state concentrations of ^{3}BDOM* and $^1O_2$ in bulk-BDOM and its molecular weight fractions with a BDOM concentration of 1 mg C per L

Steady-state concentration (10^{-15} M)	Bulk-BDOM	L-BDOM	M-BDOM	H-BDOM
$[^3\text{BDOM*}]_{ss}$	8.29	4.11	3.55	2.71
$[^1O_2]_{ss}$	8.89	8.06	6.67	5.56

with O_2 to produce $^1O_2$.[39] Accordingly, the low MW fractions of BDOM produced more $^3BDOM^*$ and $^1O_2$ than the high MW fractions, thereby playing a predominant role in enhancing 2,4-DCP indirect photodegradation.

Although all BDOM fractions promoted indirect photodegradation of 2,4-DCP ($k_{ind} > 0$), M-BDOM and H-BDOM exhibited an inhibitory effect on the overall photodegradation, except at a concentration of 2 mg C per L. This may have been because the three MW fractions of BDOM exhibited different light screening effects. As shown in the UV-vis spectrum, BDOM fractions with higher MW values exhibited stronger absorption than the smaller MW fractions. The $\sum S_\lambda$ values listed in Table 1 followed the order of L-BDOM > M-BDOM > H-BDOM at the same concentration. These results indicate that the high MW fractions of BDOM induced a stronger light screening effect than the low MW fractions, which was responsible for the inhibited overall photodegradation of 2,4-DCP.[39,61]
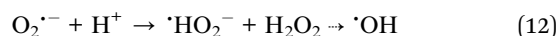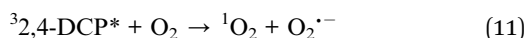
Furthermore, the phenolic compounds in BDOM could be the main quenching moieties of ROS, which are the major electron-donating moieties and positively correlated with their EDCs.[62,63] Therefore, we calculated the EDC values of bulk-BDOM and its MW fractions using the mediated electrochemistry method. Fig. S4† shows the typical current–time (i–t) responses of bulk-BDOM and its MW fractions. The higher peak area observed for L-BDOM indicates higher electron transfer numbers than bulk-BDOM and M-/H-BDOM. The EDC values of BDOM (Fig. 7d) were calculated to be 3.31–6.49 mmol $(g\ C)^{-1}$, which followed the other previously reported value for BDOM.[64] The EDC values followed the order of L-BDOM > M-BDOM > H-BDOM, indicating that L-BDOM had higher electron-donating moieties. This result implies that the lower MW fractions of BDOM contained more phenolic compounds, which may significantly inhibit the photodegradation of 2,4-DCP at high BDOM concentrations.

3.5 Possible routes for 2,4-DCP photodegradation in biochar-related environments
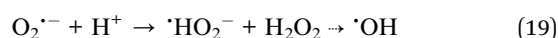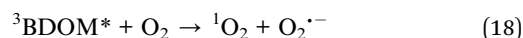
The possible routes for 2,4-DCP photodegradation based on the above results were proposed in the following three cases:

Case 1: under dark conditions, the degradation of 2,4-DCP has not occurred.

Case 2: under UV irradiation without BDOM, 2,4-DCP was excited to the singlet-excited state (^{1}2,4-DCP*) after absorbing a photon, followed by a transition to the triplet state (^{3}2,4-DCP*) (eqn (8) and (9)). Then, ^{3}2,4-DCP* underwent direct photolysis (eqn (10)) or reacted with dissolved oxygen to produce $^1O_2$ and $O_2^{\cdot-}$, which ultimately induced the production of $^{\cdot}OH$ (eqn (11) and (12)).[32] The produced $^1O_2$ and $^{\cdot}OH$ reacted with 2,4-DCP in turn, resulting in the self-sensitized photodegradation of 2,4-DCP (eqn (13) and (14)). The direct photolysis and self-sensitized photodegradation routes were supported by the findings of the inhibitory effect of 2,4-DCP by FFA and IPA in pure water.

$$2,4\text{-DCP} + UV \rightarrow {}^1 2,4\text{-DCP}^* \tag{8}$$

$$^1 2,4\text{-DCP}^* \rightarrow {}^3 2,4\text{-DCP}^* \tag{9}$$

$$^3 2,4\text{-DCP}^* \rightarrow \text{direct photolysis} \tag{10}$$

$$^3 2,4\text{-DCP}^* + O_2 \rightarrow {}^1O_2 + O_2^{\cdot-} \tag{11}$$

$$O_2^{\cdot-} + H^+ \rightarrow {}^{\cdot}HO_2^- + H_2O_2 \dashrightarrow {}^{\cdot}OH \tag{12}$$

$$^1O_2 + 2,4\text{-DCP} \rightarrow \text{self-photodegradation} \tag{13}$$

$$^{\cdot}OH + 2,4\text{-DCP} \rightarrow \text{self-photodegradation} \tag{14}$$

Case 3: under UV irradiation in the presence of BDOM, BDOM was excited to its singlet-excited state ($^1BDOM^*$) and then formed $^3BDOM^*$ through intersystem crosses (eqn (15) and (16)). The $^3BDOM^*$ molecules reacted with 2,4-DCP via both electron and energy transfer pathways (eqn (17)). This process was supported by the results of the quenching experiments, which showed that SA and TMP induced a similar inhibitory efficiency in BDOM-mediated 2,4-DCP photodegradation. Additionally, the dissolved oxygen in the solution reacted with $^3BDOM^*$ through electron transfer, resulting in the generation of $^1O_2$ and $^{\cdot}OH$ (eqn (18) and (19)). The $^1O_2$ played a secondary role in the indirect photodegradation of 2,4-DCP mediated by BDOM, whereas the roles of other ROS, such as $^{\cdot}OH$, were insignificant (eqn (20) and (21)). Therefore, it can be concluded that BDOM released in biochar-related environments affects the photodegradation process of 2,4-DCP by two mechanisms. Initially, UV irradiation induces the excitation of BDOM to $^3BDOM^*$, which directly mediates the degradation of 2,4-DCP through both electron transfer and energy transfer mechanisms. Simultaneously, the produced $^3BDOM^*$ triggers the formation of ROS, such as $^1O_2$ and $^{\cdot}OH$, which subsequently oxidize and degrade 2,4-DCP.

$$BDOM + UV \rightarrow {}^1BDOM^* \tag{15}$$

$$^1BDOM^* \rightarrow {}^3BDOM^* \tag{16}$$

$$^3BDOM^* + 2,4\text{-DCP} \rightarrow \text{photodegradation} \tag{17}$$

$$^3BDOM^* + O_2 \rightarrow {}^1O_2 + O_2^{\cdot-} \tag{18}$$

$$O_2^{\cdot-} + H^+ \rightarrow {}^{\cdot}HO_2^- + H_2O_2 \dashrightarrow {}^{\cdot}OH \tag{19}$$

$$^1O_2 + 2,4\text{-DCP} \rightarrow \text{photodegradation} \tag{20}$$

$$^{\cdot}OH + 2,4\text{-DCP} \rightarrow \text{photodegradation} \tag{21}$$

To illustrate the photodegradation pathways of 2,4-DCP, the possible intermediate products generated during the 2,4-DCP photodegradation process were analyzed using GC/MS technique. As listed in Table S4,† a total of five intermediate products were determined after photodegradation for 30 h, including 3,5-dichlorocatechol, 2-chlorophenol, hydroquinone, maleic acid and oxalic acid. Considering the results of GC/MS and the insights from previous studies,[65,66] the possible degradation pathways of 2,4-DCP were proposed in Fig. 8. Conversely, 2,4-DCP could be attacked by $^3BDOM^*$, $^1O_2$ and/or $^{\cdot}OH$ at the para-position of a chlorine atom to form 2-chlorophenol by the dechlorination reaction.[67] In contrast, 2,4-DCP could be
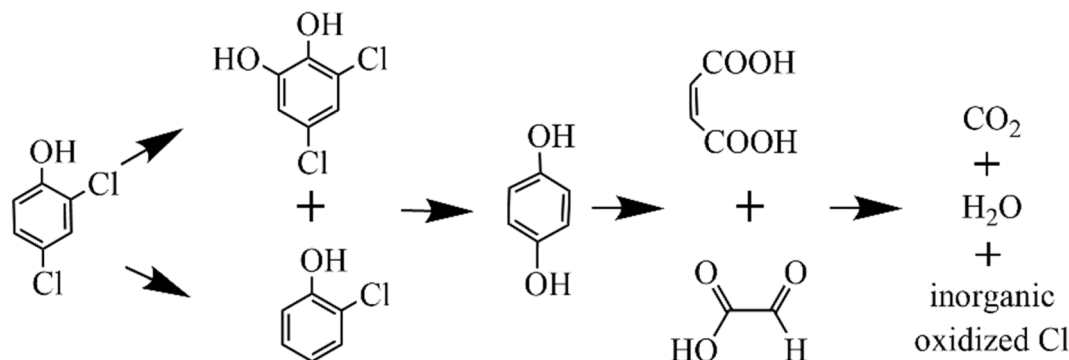
Fig. 8 Possible photodegradation pathways of 2,4-DCP.

converted by $\cdot$OH into its hydroxylation product, 3,5-dichlorocatechol. These intermediates were further degraded by ROS into hydroquinone, which subsequently underwent ring-opening to form maleic acid and oxalic acid.[68] Finally, these low MW organic acids were further oxidized and mineralized to CO_2.

Furthermore, the photodegradation process of 2,4-DCP mediated by BDOM was influenced by concentrating BDOM and its MW. BDOM enhanced the indirect photodegradation of 2,4-DCP, and this facilitation effect was weakened with BDOM concentrations because of the amplified light screening effect and the scavenging of ROS by phenolic moieties. The low MW fractions of BDOM contributed more to 2,4-DCP indirect photodegradation because of their higher potential for ROS production than the high MW fractions. However, the high MW fractions of BDOM displayed a higher light screen effect than the low MW fractions, resulting in an inhibitory effect on the overall photodegradation of 2,4-DCP. Additionally, UV irradiation is a key factor in triggering the photodegradation of 2,4-DCP; thus, the intensity and wavelength of UV radiation could significantly influence 2,4-DCP photodegradation, which should be further studied in our future work.

4. Conclusion

In this study, we evaluated the impacts of BDOM from crop residue-derived biochar and its MW fractions on 2,4-DCP photodegradation. It was found that 2,4-DCP photodegradation in the presence of BDOM may occur *via* direct photolysis, self-sensitization photolysis, and indirect photodegradation mediated by $^3BDOM^*$, $^1O_2$ and $\cdot$OH. The impacts of BDOM on 2,4-DCP photodegradation depended on the BDOM concentration and MW fraction. BDOM facilitated the photodegradation of 2,4-DCP by generating $^3BDOM^*$, $^1O_2$ and $\cdot$OH, which contributed 60%, 22.2% and 4.4% to total 2,4-DCP photodegradation, respectively. However, increasing the BDOM concentration decelerates the photodegradation of 2,4-DCP because of the amplified light screening effect and the scavenging of ROS by the phenolic moieties. The lower MW fractions in BDOM had a higher potential to produce $^3BDOM^*$, $^1O_2$ and $\cdot$OH compared to the high MW fractions, thereby contributing more significantly to promoting the photodegradation of 2,4-DCP. However,

the high MW fractions of BDOM exhibited a greater light screening effect, which hindered the photodegradation of 2,4-DCP.

Data availability

The data underlying this study are available in the article and ESI.†

Conflicts of interest

The authors declare no conflicts of interest.

Acknowledgements

References

1 Z. Gu, N. Ni, G. He, Y. Shan, K. Wu, C. Hu and J. Qu, Enhanced hydrosaturation selectivity and electron transfer for electrocatalytic chlorophenols hydrogenation on Ru sites, *Environ. Sci. Technol.*, 2023, **57**, 16695–16706, DOI: **10.1021/acs.est.3c06669**.

2 A. H. Kamel, H. S. M. Abd-Rabboh and A. Hefnawy, Molecularly imprinted polymer-based electrochemical sensors for monitoring the persistent organic pollutants chlorophenols, *RSC Adv.*, 2024, **14**, 20163–20181, DOI: **10.1039/d4ra03095h**.

3 J. Jiang, H. Zhao, D. Xia, X. Li and B. Qu, Formation of free radicals by direct photolysis of halogenated phenols (HPs) and effects of DOM: a case study on monobromophenols, *J. Hazard. Mater.*, 2020, **391**, 122220, DOI: **10.1016/j.jhazmat.2020.122220**.

4 Q. Tian, S. Chen, J. Yu, M. Zhang, N. Gao, X. Yang, C. Wang, X. Duan and L. Zang, Tunable construction of electrochemical sensors for chlorophenol detection, *J.*

Mater. Chem. C, 2022, **10**, 10171–10195, DOI: **10.1039/d2tc01369j**.

5 S. Yadav, S. Kumar and A. K. Haritash, A comprehensive review of chlorophenols: fate, toxicology and its treatment, *J. Environ. Manage.*, 2023, **342**, 118254, DOI: **10.1016/j.jenvman.2023.118254**.

6 T. T. Tran-Lam, T. C. Quan, P. T. Pham, A. T. T. Phung, M. Q. Bui and Y. H. Dao, Occurrence, distribution, and risk assessment of halogenated organic pollutants (HOPs) in marine fish muscle: the case study of Vietnam, *Mar. Pollut. Bull.*, 2023, **192**, 114986, DOI: **10.1016/j.marpolbul.2023.114986**.

7 A. Y. Sholokhova, S. A. Borovikova and D. D. Matyushin, Refinement of retention indices in gas chromatography for a number of substituted phenols, *Analytica*, 2024, **5**, 641–653, DOI: **10.3390/analytica5040043**.

8 B. Wu, W. A. Arnold and L. Ma, Photolysis of atrazine: role of triplet dissolved organic matter and limitations of sensitizers and quenchers, *Water Res.*, 2021, **190**, 116659, DOI: **10.1016/j.watres.2020.116659**.

9 J. Yoon, D. Tokmurzin, D. Lee, S. Hoon, M. Won and Y. Park, Production of biochar from crop residues and its application for biofuel production processes - an overview, *Bioresour. Technol.*, 2022, **361**, 127740, DOI: **10.1016/j.biortech.2022.127740**.

10 R. Shinde, D. Kumar, P. Mahapatra, C. Shekhar, S. Kumar, N. Thombare and A. Kumar, Management of crop residues with special reference to the on-farm utilization methods: a review, *Ind. Crops Prod.*, 2022, **181**, 114772, DOI: **10.1016/j.indcrop.2022.114772**.

11 H. Wang, J. Xu and L. Sheng, Preparation of straw biochar and application of constructed wetland in China: a review, *J. Clean. Prod.*, 2020, **273**, 123131, DOI: **10.1016/j.jclepro.2020.123131**.

12 J. Lehmann, A. Cowie, C. A. Masiello, C. Kammann, D. Woolf, J. E. Amonette, M. L. Cayuela, M. Camps-Arbestain and T. Whitman, Biochar in climate change mitigation, *Nat. Geosci.*, 2021, **14**, 883–892, DOI: **10.1038/s41561-021-00852-8**.

13 M. Hu, L. Hu, X. Miao, L. Duan, L. Jiang, H. Zhu, W. Wu, D. Lin and K. Yang, Selective degradation of KOH activated biochar adsorbed 4-chlorophenol with fulvic acid by peroxydisulfate, *J. Environ. Chem. Eng.*, 2025, **13**, 116062, DOI: **10.1016/j.jece.2025.116062**.

14 X. Yao, X. Chen, M. Chen, N. Feng, L. Tong, Y. Yi, W. Qian and Z. Diao, Removal of pesticide acetamiprid using KOH activated biochar derived from crayfish shell: behavior and mechanism, *Process Saf. Environ. Prot.*, 2024, **186**, 808–818, DOI: **10.1016/j.psep.2024.04.076**.

15 I. M. Radwan, C. Wang, J. Kim, H. Wei and D. Wang, Sorptive removal of neonicotinoid pesticides by nanobiochars: efficiency, kinetics, and reusability, *J. Hazard. Mater.*, 2025, **493**, 138354, DOI: **10.1016/j.jhazmat.2025.138354**.

16 C. Liu, H. Wang, P. Li, Q. Xian and X. Tang, Biochar's impact on dissolved organic matter (DOM) export from a cropland soil during natural rainfalls, *Sci. Total Environ.*, 2019, **650**, 1988–1995, DOI: **10.1016/j.scitotenv.2018.09.356**.

17 Y. Tian, L. Feng, C. Wang, Y. Liu, J. Zou, R. Li, Z. Du and L. Zhang, Dissolved black carbon enhanced the aquatic photo-transformation of chlortetracycline via triplet excited-state species: the role of chemical composition, *Environ. Res.*, 2019, **179**, 108855, DOI: **10.1016/j.envres.2019.108855**.

18 B. K. Biswal, K. Vijayaraghavan, D. L. Tsen-Tieng and R. Balasubramanian, Biochar-based bioretention systems for removal of chemical and microbial pollutants from stormwater: a critical review, *J. Hazard. Mater.*, 2022, **422**, 126886, DOI: **10.1016/j.jhazmat.2021.126886**.

19 M. Haris, Y. Hamid, M. Usman, L. Wang, A. Saleem, F. Su, J. K. Guo and Y. Li, Crop-residues derived biochar: synthesis, properties, characterization and application for the removal of trace elements in soils, *J. Hazard. Mater.*, 2021, **416**, 126212, DOI: **10.1016/j.jhazmat.2021.126212**.

20 X. Huang, B. Xu, S. Zhu, F. Ma and C. Jin, Overlooked contributions of biochar-derived dissolved organic matter on the adsorption of Pb(II): impacts of fractionation and interfacial force, *J. Hazard. Mater.*, 2021, **420**, 126692, DOI: **10.1016/j.jhazmat.2021.126692**.

21 N. Kaur, C. Kieffer, W. Ren and D. Hui, How much is soil nitrous oxide emission reduced with biochar application? An evaluation of meta-analyses, *GCB Bioenergy*, 2023, **15**, 24–37, DOI: **10.1111/gcbb.13003**.

22 R. Ji, Y. Yang, Y. Wu, C. Zhu, J. Min, C. Liu, L. Zhang, H. Cheng, J. Xue and D. Zhou, Capturing differences in the release potential of dissolved organic matter from biochar and hydrochar: insights from component characterization and molecular identification, *Sci. Total Environ.*, 2024, **955**, 177209, DOI: **10.1016/j.scitotenv.2024.177209**.

23 Q. Lang, X. Guo, C. Wang, L. Li, Y. Li, J. Xu, X. Zhao, J. Li, B. Liu, Q. Sun and G. Zou, Characteristics and phytotoxicity of hydrochar-derived dissolved organic matter: effects of feedstock type and hydrothermal temperature, *J. Environ. Sci.*, 2025, **149**, 139–148, DOI: **10.1016/j.jes.2023.10.007**.

24 Y. Ye, X. Cai, Z. Wang and X. Xie, Characterization of dissolved black carbon and its binding behaviors to ceftazidime and diclofenac pharmaceuticals: employing the molecular weight fractionation, *Environ. Pollut.*, 2022, **315**, 120449, DOI: **10.1016/j.envpol.2022.120449**.

25 H. Fu, H. Liu, J. Mao, W. Chu, Q. Li, P. J. J. Alvarez, X. Qu and D. Zhu, Photochemistry of dissolved black carbon released from biochar: reactive oxygen species generation and phototransformation, *Environ. Sci. Technol.*, 2016, **50**, 1218–1226, DOI: **10.1021/acs.est.5b04314**.

26 Z. Zhou, B. Chen, X. Qu, H. Fu and D. Zhu, Dissolved black carbon as an efficient sensitizer in the photochemical transformation of 17β-estradiol in aqueous solution, *Environ. Sci. Technol.*, 2018, **52**, 10391–10399, DOI: **10.1021/acs.est.8b01928**.

27 X. Z. Niu, F. Busetti, M. Langsa and J. P. Croué, Roles of singlet oxygen and dissolved organic matter in self-sensitized photo-oxidation of antibiotic norfloxacin under sunlight irradiation, *Water Res.*, 2016, **106**, 214–222, DOI: **10.1016/j.watres.2016.10.002**.

28 J. Wenk and S. Canonica, Phenolic antioxidants inhibit the triplet-induced transformation of anilines and sulfonamide antibiotics in aqueous solution, *Environ. Sci.*, 2012, **46**, 5455–5462, DOI: **10.1021/es300485u**.

29 X. Xu, H. Huang, Y. Zhang, Z. Xu and X. Cao, Biochar as both electron donor and electron shuttle for the reduction transformation of Cr(VI) during its sorption, *Environ. Pollut.*, 2019, **244**, 423–430, DOI: **10.1016/j.envpol.2018.10.068**.

30 F. Yang, C. Wang and H. Sun, A comprehensive review of biochar-derived dissolved matters in biochar application: production, characteristics, and potential environmental effects and mechanisms, *J. Environ. Chem. Eng.*, 2021, **9**, 105258, DOI: **10.1016/j.jece.2021.105258**.

31 V. K. H. Bui, X. C. Nguyen and J. Hur, Revisiting triplet state dissolved organic matter (^{3}DOM*): advances in probes, photoreactivity, and environmental implications, *Sci. Total Environ.*, 2024, **954**, 176226, DOI: **10.1016/j.scitotenv.2024.176226**.

32 W. Ma, J. He, L. Han, C. Ma, Y. Cai, X. Guo and Z. Yang, Hydrophilic fraction of dissolved organic matter largely facilitated microplastics photoaging: insights from redox properties and reactive oxygen species, *Environ. Sci. Technol.*, 2024, **58**, 11625–11636, DOI: **10.1021/acs.est.3c11111**.

33 K. Yang, Y. Zhang, J. Peng, H. Xu, X. Liu, H. Liu, N. Li, L. Guo and W. Li, Molecular weight-dependent differences in spectral properties and metal-binding behaviors of dissolved organic matter from different lakes, *Sci. Total Environ.*, 2024, **946**, 174245, DOI: **10.1016/j.scitotenv.2024.174245**.

34 C. W. Cuss and C. Guéguen, Determination of relative molecular weights of fluorescent components in dissolved organic matter using asymmetrical flow field-flow fractionation and parallel factor analysis, *Anal. Chim. Acta*, 2012, **733**, 98–102, DOI: **10.1016/j.aca.2012.05.003**.

35 H. Zhang, L. Wu, W. Qian, J. Ni, R. Wei, Z. Qi and W. Chen, Spectral characteristics of dissolved organic carbon derived from biomass-pyrogenic smoke (SDOC) in the aqueous environment and its solubilization effect on hydrophobic organic pollutants, *Water Res.*, 2021, **203**, 117515, DOI: **10.1016/j.watres.2021.117515**.

36 S. Yu, H. Zhang, J. Ni, Y. Xiang, R. Wei, W. Qian and W. Chen, Spectral characteristics coupled with self-organizing maps analysis on different molecular size-fractionated water-soluble organic carbon from biochar, *Sci. Total Environ.*, 2023, **857**, 159424, DOI: **10.1016/j.scitotenv.2022.159424**.

37 W. Wang, M. Nie, C. Yan, Y. Yuan, A. Xu, M. Ding, P. Wang and M. Ju, Effect of pyrolysis temperature and molecular weight on characterization of biochar derived dissolved organic matter from invasive plant and binding behavior with the selected pharmaceuticals, *Environ. Pollut.*, 2024, **348**, 123867, DOI: **10.1016/j.envpol.2024.123867**.

38 H. Liu, Y. Wang, S. Wang, J. Wu and Y. Wang, Release characteristics of biochar-derived dissolved organic matter and its impact on Cr(VI) adsorption and reduction, *RSC Adv.*, 2024, **14**, 38171–38182, DOI: **10.1039/d4ra06172a**.

39 S. Liu, Z. Cui, D. Ding, Y. Bai, J. Chen, H. Cui, R. Su and K. Qu, Effect of the molecular weight of DOM on the indirect photodegradation of fluoroquinolone antibiotics, *J. Environ. Manag.*, 2023, **348**, 119192, DOI: **10.1016/j.jenvman.2023.119192**.

40 Y. Wang, Y. Gao, T. Ye, Y. Hu and C. Yang, Dynamic variations of dissolved organic matter from treated wastewater effluent in the receiving water: photo- and bio-degradation kinetics and its environmental implications, *Environ. Res.*, 2021, **194**, 110709, DOI: **10.1016/j.envres.2021.110709**.

41 J. Wenk, U. Von Gunten and S. Canonica, Effect of dissolved organic matter on the transformation of contaminants induced by excited triplet states and the hydroxyl radical, *Environ. Sci. Technol.*, 2011, **45**, 1334–1340, DOI: **10.1021/es102212t**.

42 S. Liu, Z. Cui, Y. Bai, D. Ding, Q. Hu, Y. Wei, L. Zhu, K. Qu and R. Su, Optical characteristic of dissolved organic matter polar fractions by spectrum technologies and the relationship with indirect photodegradation of ofloxacin, *J. Environ. Chem. Eng.*, 2024, **12**, 114371, DOI: **10.1016/j.jece.2024.114371**.

43 A. P. S. Batista, A. C. Teixeira, W. J. Cooper and B. A. Cottrell, Correlating the chemical and spectroscopic characteristics of natural organic matter with the photodegradation of sulfamerazine, *Water Res.*, 2016, **93**, 20–29, DOI: **10.1016/j.watres.2015.11.036**.

44 E. Appiani, R. Ossola, D. E. Latch, P. R. Erickson and K. McNeill, Aqueous singlet oxygen reaction kinetics of furfuryl alcohol: effect of temperature, pH, and salt content, *Environ. Sci.: Processes Impacts*, 2017, **19**, 507–516, DOI: **10.1039/c6em00646a**.

45 L. Klüpfel, M. Keiluweit, M. Kleber and M. Sander, Redox properties of plant biomass-derived black carbon (biochar), *Environ. Sci. Technol.*, 2014, **48**, 5601–5611, DOI: **10.1021/es500906d**.

46 B. Zhang, S. Zhou, L. Zhou, J. Wen and Y. Yuan, Pyrolysis temperature-dependent electron transfer capacities of dissolved organic matters derived from wheat straw biochar, *Sci. Total Environ.*, 2019, **696**, 133895, DOI: **10.1016/j.scitotenv.2019.133895**.

47 A. Michael, S. Michael and P. S. René, Novel electrochemical approach to assess the redox properties of humic substances, *Environ. Sci. Technol.*, 2010, **44**, 87–93, DOI: **10.1021/es902627p**.

48 M. H. Hsu, C. J. Tsai and A. Y. C. Lin, Mechanism and pathways underlying the self-sensitized photodegradation of methotrexate under simulated solar irradiation, *J. Hazard. Mater.*, 2019, **373**, 468–475, DOI: **10.1016/j.jhazmat.2019.03.095**.

49 X. Xie, Z. Zhang, Y. Hu and H. Cheng, A mechanistic kinetic model for singlet oxygen mediated self-sensitized photo-oxidation of organic pollutants in water, *Chem. Eng. J.*, 2018, **334**, 1242–1251, DOI: **10.1016/j.cej.2017.11.070**.

© 2025 The Author(s). Published by the Royal Society of Chemistry

50 Y. Fu, Y. Yan, Z. Wei, R. Spinney, D. D. Dionysiou, D. Vione, M. Liu and R. Xiao, Overlooked transformation of nitrated polycyclic aromatic hydrocarbons in natural waters: role of self-photosensitization, *Environ. Sci. Technol.*, 2023, **57**, 9832–9842, DOI: **10.1021/acs.est.3c02276**.

51 H. Luo, E. Almatrafi, W. Wang, Y. Yang, D. Huang, W. Xiong, M. Cheng, C. Zhou, Y. Zhou, Q. Lin, G. Fang, G. Zeng and C. Zhang, Insight into the effect of pyrolysis temperature on photoreactivity of biochar-derived dissolved organic matter: impacts of aromaticity and carbonyl groups, *Sci. Total Environ.*, 2023, **871**, 162048, DOI: **10.1016/j.scitotenv.2023.162048**.

52 Y. Bai, Y. Zhou, X. Che, C. Li, Z. Cui, R. Su and K. Qu, Indirect photodegradation of sulfadiazine in the presence of DOM: effects of DOM components and main seawater constituents, *Environ. Pollut.*, 2021, **268**, 115689, DOI: **10.1016/j.envpol.2020.115689**.

53 J. Wang, K. Wang, Y. Guo and J. Niu, Photochemical degradation of nebivolol in different natural organic matter solutions under simulated sunlight irradiation: kinetics, mechanism and degradation pathway, *Water Res.*, 2020, **173**, 115524, DOI: **10.1016/j.watres.2020.115524**.

54 Y. Sun, X. Xiong, M. He, Z. Xu, D. Hou, W. Zhang, Y. S. Ok, J. Rinklebe, L. Wang and D. C. W. Tsang, Roles of biochar-derived dissolved organic matter in soil amendment and environmental remediation: a critical review, *Chem. Eng. J.*, 2021, **424**, 130387, DOI: **10.1016/j.cej.2021.130387**.

55 G. Fang, C. Liu, Y. Wang, D. D. Dionysiou and D. Zhou, Photogeneration of reactive oxygen species from biochar suspension for diethyl phthalate degradation, *Appl. Catal., B*, 2017, **214**, 34–45, DOI: **10.1016/j.apcatb.2017.05.036**.

56 J. Pan, S. Zhang, X. Qiu, L. Ding, X. Liang and X. Guo, Molecular weights of dissolved organic matter significantly affect photoaging of microplastics, *Environ. Sci. Technol.*, 2024, **58**, 13973–13985, DOI: **10.1021/acs.est.4c04608**.

57 K. J. Moor, M. Schmitt, P. R. Erickson and K. McNeill, Sorbic acid as a triplet probe: triplet energy and reactivity with triplet-state dissolved organic matter via $^1O_2$ phosphorescence, *Environ. Sci. Technol.*, 2019, **53**, 8078–8086, DOI: **10.1021/acs.est.9b01787**.

58 Y. Kang, Z. Chu, X. Xie, L. Li, J. Hu, S. Li and Z. Wang, Variation in photoactivity of dissolved black carbon during the fractionation process and the role in the photodegradation of various antibiotics, *J. Hazard. Mater.*, 2024, **480**, 136435, DOI: **10.1016/j.jhazmat.2024.136435**.

59 H. Zhang, W. Qian, L. Wu, S. Yu, R. Wei, W. Chen and J. Ni, Spectral characteristics of dissolved organic carbon (DOC) derived from biomass pyrolysis: biochar-derived DOC versus smoke-derived DOC, and their differences from natural DOC, *Chemosphere*, 2022, **302**, 134869, DOI: **10.1016/j.chemosphere.2022.134869**.

60 C. H. Liu, W. Chu, H. Li, S. A. Boyd, B. J. Teppen, J. Mao, J. Lehmann and W. Zhang, Quantification and characterization of dissolved organic carbon from biochars, *Geoderma*, 2019, **335**, 161–169, DOI: **10.1016/j.geoderma.2018.08.019**.

61 C. Zhou, Q. Xie, J. Wang, X. Chen, J. Niu and J. Chen, Effects of dissolved organic matter derived from freshwater and seawater on photodegradation of three antiviral drugs, *Environ. Pollut.*, 2020, **258**, 113700, DOI: **10.1016/j.envpol.2019.113700**.

62 J. Lv, R. Han, Z. Huang, L. Luo, D. Cao and S. Zhang, Relationship between molecular components and reducing capacities of humic substances, *ACS Earth Space Chem.*, 2018, **2**, 330–339, DOI: **10.1021/acsearthspacechem.7b00155**.

63 Y. Zhang, X. Xu, L. Cao, Y. S. Ok and X. Cao, Characterization and quantification of electron donating capacity and its structure dependence in biochar derived from three waste biomasses, *Chemosphere*, 2018, **211**, 1073–1081, DOI: **10.1016/j.chemosphere.2018.08.033**.

64 J. Wang, J. Chen, X. Qiao, Y. N. Zhang, M. Uddin and Z. Guo, Disparate effects of DOM extracted from coastal seawaters and freshwaters on photodegradation of 2,4-dihydroxybenzophenone, *Water Res.*, 2019, **151**, 280–287, DOI: **10.1016/j.watres.2018.12.045**.

65 Z. Diao, L. Yan, F. Dong, W. Qian, Q. Deng, L. Kong, J. Yang, Z. Lei, J. Du and W. Chu, Degradation of 2,4-dichlorophenol by a novel iron based system and its synergism with Cd(II) immobilization in a contaminated soil, *Chem. Eng. J.*, 2020, **379**, 122313, DOI: **10.1016/j.cej.2019.122313**.

66 Z. Diao, Z. Lin, X. Chen, L. Yan, F. Dong, W. Qian, L. Kong, J. Du and W. Chu, Ultrasound-assisted heterogeneous activation of peroxymonosulphate by natural pyrite for 2,4-diclorophenol degradation in water: synergistic effects, pathway and mechanism, *Chem. Eng. J.*, 2020, **389**, 123771, DOI: **10.1016/j.cej.2019.123771**.

67 Y. Han, M. Tai, Y. Yao, J. Li, Y. Wu, B. Hu, Y. Ma and C. Liu, Iron-decorated covalent organic framework as efficient catalyst for activating peroxydisulfate to degrade 2,4-dichlorophenol: performance and mechanism insight, *J. Colloid Interface Sci.*, 2024, **663**, 238–250, DOI: **10.1016/j.jcis.2024.02.165**.

68 M. Hao, Q. Wang, F. Yu, Z. Guan, X. Zhang and Y. Sun, Efficient degradation of 2,4-dichlorophphenol in groundwater using persulfate activated by nitrogen-doped biochar-supported nano zero-valent iron, *J. Clean. Prod.*, 2024, **458**, 142415, DOI: **10.1016/j.jclepro.2024.142415**.